

Experimental Phase-Matching Quantum Cryptographic Conferencing in Symmetric and Asymmetric Fiber Channels

Mi Zou,¹ Bin-Chen Li,^{1, 2, 3} Shuai Zhao,^{4, 5} Yingqiu Mao,^{2, 6} Dandan Qin,^{1, 2, 3} Xiao Jiang,^{1, 2, 3} Teng-Yun Chen,^{1, 2, 3, *} and Jian-Wei Pan^{1, 2, 3, †}

¹Hefei National Laboratory, University of Science and Technology of China, Hefei 230088, China

²Hefei National Research Center for Physical Sciences at the Microscale and School of Physical Sciences, University of Science and Technology of China, Hefei 230026, China

³CAS Center for Excellence in Quantum Information and Quantum Physics, University of Science and Technology of China, Hefei 230026, China

⁴School of Cyberspace, Hangzhou Dianzi University, Hangzhou 310018, China

⁵Pinghu Digital Technology Innovation Research Institute, Hangzhou Dianzi University, Pinghu, 314200, China

⁶Shanghai Research Center for Quantum Science and CAS Center for Excellence in Quantum Information and Quantum Physics, University of Science and Technology of China, Shanghai 201315, China

Quantum cryptographic conferencing (QCC) allows multiple parties to establish common secure keys in quantum networks with information-theoretic security. However, the secure transmission distances of current QCC implementations are still limited to the metropolitan areas. Here, we experimentally demonstrate the three-intensity phase-matching (PM) QCC protocol considering finite-size effects by employing frequency-locking and phase-tracking techniques for three parties. The key distribution capability of the PM QCC protocol is demonstrated in the symmetric fiber channels with the distance from each party to the measurement site up to 100 km. The network adaptability of the PM QCC protocol is demonstrated in asymmetric fiber channels used to simulate fiber channel configurations in real networks. Thus, the feasibility of applying the PM QCC protocol to practical intercity quantum networks with both symmetric and asymmetric channels is verified.

I. INTRODUCTION

Quantum networks aim to achieve information processing tasks beyond the capabilities of classical networks [1–3], with quantum key distribution (QKD) being a key application that enables secure key generation between remote parties [4, 5]. Various QKD networks, featuring different topologies and scales, have been developed to enhance the practical use of quantum information [6–12]. When multiple parties in a network intend to generate a common secure key, the approach using bipartite QKD protocols requires either one party to generate independent identical secure key pairs with each of the remaining parties individually or adjacent parties to generate their own independent identical secure key pairs between themselves. These pairwise keys are then converted into a multi-party common key via classical XOR operations. An alternative, more concise and efficient approach is to directly generate a multi-party common secure key by leveraging multipartite entanglement [13–25].

Figure 1 depicts a star-type quantum network application facilitating an encrypted conference among three parties using the quantum cryptographic conferencing (QCC) protocol, which generates secure common keys. This protocol can utilize either an entanglement-based approach that distributes the genuine multi-party entan-

gled state [13, 15, 16] or time-reversal methods that post-select the Greenberger-Horne-Zeilinger (GHZ)[14, 19, 24] or W states [17, 23]. While the entanglement-based QCC is limited by the fragility of multi-party entangled states [26, 27], the time-reversal QCC, employing weak coherent states, offers greater practicality and is resistant to detector side-channel attacks, making it measurement-device-independent (MDI). Recent implementations of the MDI QCC protocol, based on polarization encoding, have achieved secure key rates constrained by inherent transmittance limitations [28, 29]. The proposed phase-matching QCC (PM QCC) protocol [19] enhances

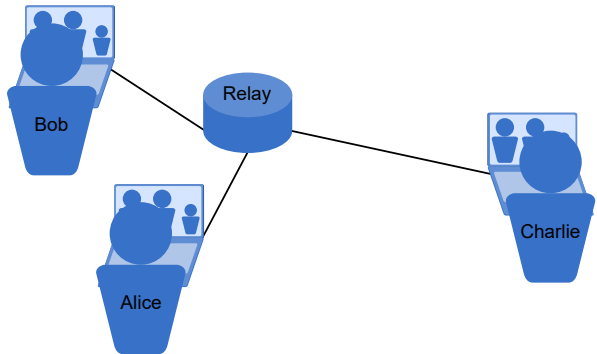


FIG. 1. Three parties in a star-type quantum network are conducting an encrypted conference using the common key generated by the QCC protocol. The relay can be an untrusted entanglement source or measurement site, and the distance from each party to the relay may be different.

* tchen@ustc.edu.cn

† pan@ustc.edu.cn

the key rate from $O(\eta^M)$ to $O(\eta^{M-1})$ with respect to the transmittance η from each party to the measurement site and the number of parties M , allowing for longer secure transmission distances. However, the original PM QCC assumes symmetric channels, while real networks often exhibit asymmetric channels, necessitating loss compensation methods to achieve symmetry.

In this work, we extend the security proof of the original PM QCC protocol to asymmetric channels, an issue of widespread concern in QKD protocols [30–37], and refine the protocol into a three-intensity scheme, which simplifies intensity modulation. In this way, the PM QCC protocol can be implemented in asymmetric channels by optimizing the transmitted light intensity of each party instead of compensating for the loss. We experimentally demonstrate the three-intensity PM QCC protocol considering finite-size effects [38] by employing frequency-locking and phase-tracking techniques for three parties. The refined PM QCC protocol is implemented in symmetric channels with the distance from each party to the measurement site increasing from 25 km to 100 km in intervals of 25 km and in five asymmetric fiber channel configurations chosen from an arrangement of 25 km, 50 km and 75 km. These results promote the application of QCC protocols in real quantum networks.

II. PROTOCOL

The three-intensity PM QCC protocol begins by Alice preparing the coherent state $|e^{i\varphi_A}\sqrt{\mu_A}\rangle$ for each round. The modulated intensity μ_A is randomly chosen from one signal-state intensity and two decoy-state intensities denoted as $\{\mu_a, \nu_a, \omega_a\}$ with probabilities $\{p_\mu, p_\nu, p_\omega\}$, where $\omega_a < \nu_a < \mu_a$, $p_\mu + p_\nu + p_\omega = 1$. The modulated phase $\varphi_A = \phi_a + \pi k_a$, where $k_a \in \{0, 1\}$ is one random bit, and ϕ_a is randomly chosen from $\{0, \frac{2\pi}{D}, \frac{4\pi}{D}, \dots, \frac{2\pi(D-1)}{D}\}$. Here, D is the number of phase slices. Similarly, Bob (Charlie) prepares the coherent state $|e^{i\varphi_B}\sqrt{\mu_B}\rangle$ ($|e^{i\varphi_C}\sqrt{\mu_C}\rangle$) with the intensity $\mu_B \in \{\mu_b, \nu_b, \omega_b\}$ ($\mu_C \in \{\mu_c, \nu_c, \omega_c\}$) and the phase $\varphi_B = \phi_b + \pi k_b$ ($\varphi_C = \phi_c + \pi k_c$). Here, k_b (k_c) is a random bit similar to k_a , and ϕ_b (ϕ_c) is a random phase similar to ϕ_a . They then send their coherent states to the untrusted measurement site, Eve. An honest Eve splits Alice's coherent state into two parts to interfere with Bob and Charlie's coherent states, respectively. Thus, two measurement branches are created, followed by two single photon detectors in each branch. Then Eve records the successful detection event, i.e., only one detector click for each measurement branch in that round.

After repeating the above procedure for many rounds, Eve announces all the successful detection events, Alice, Bob, and Charlie announce their random phases and intensities and perform the sifting step to obtain raw keys. They retain or flip their random bits only when the following phase-matching conditions are satisfied: $|\phi_a - \phi_b| = 0$ or π , $|\phi_a - \phi_c| = 0$ or π ; and the intensities of coherent states they prepared are $\{\mu_a, \mu_b, \mu_c\}$, $\{\nu_a, \nu_b, \nu_c\}$, or $\{\omega_a, \omega_b, \omega_c\}$, respectively. The secure keys are obtained by performing parameter estimation and key distillation. The security proof of the protocol is realized via entanglement-based method [19] and source replacement method [39] (see Appendix A for more details). The key rate of the three-intensity PM QCC protocol for three parties can be expressed as

$$R = \left(\frac{2}{D}\right)^2 Q_\mu [1 - fh(E_Z^{\max}) - h(E_X^U)], \quad (1)$$

where $(2/D)^2$ is the prefactor induced by phase post-selection, Q_μ is the gain of signal state, f is the error correction efficiency, $h(x) = -x \log_2(x) - (1-x) \log_2(1-x)$ is the binary entropy function. E_Z^{\max} is the maximum value between E_Z^{AB} and E_Z^{AC} , where E_Z^{AB} (E_Z^{AC}) is the quantum bit error rate between Alice and Bob (Charlie), which can be directly obtained from the experimental results. E_X^U is the upper bound of the phase error rate, which can be estimated by decoy-state method given in Appendix A.

III. EXPERIMENT

The three-intensity PM QCC protocol is implemented with the setup shown in Fig. 2. All three parties have coherent light sources (CLSs) and encoders for coherent state preparation. To establish a stable phase reference between three parties, they first need to ensure that their CLSs have the same frequency. To this end, the continuous-wave laser (CWL) of Alice is used as the master CWL (MCWL) to send out two beams of frequency reference light. Bob and Charlie receive two frequency reference beams from Alice and lock their slave CWLs to them. They use heterodyne optical phase-locked loop technology [40] to make a stable 50 MHz frequency difference between their CLSs and the frequency reference light. Due to the bandwidth limitation of the piezo actuator of the laser for frequency locking, an acousto-optic modulator is inserted to increase the feedback bandwidth of the loop. In this way, two CLSs of Bob and Charlie have the same frequency, but are 50 MHz different from the Alice's MCWL. Thus, Alice needs to frequency shift her coherent light by 50 MHz with an acousto-optic modulator, so that the frequency of her CLS is the same as that of Bob's and Charlie's. Note that the MCWL is placed at Alice's end to simplify the demonstration. For geographically separated parties, it can instead be deployed at the measurement site, with the generated frequency reference beams transmitted to each party via additional optical fibers to enable frequency locking.

The encoders are the same for all three parties and are used to achieve weak coherent pulse (WCP) generation, pulse intensity modulation and phase modulation. The generation of coherent light pulses is realized by an intensity modulator, which converts continuous wave into light

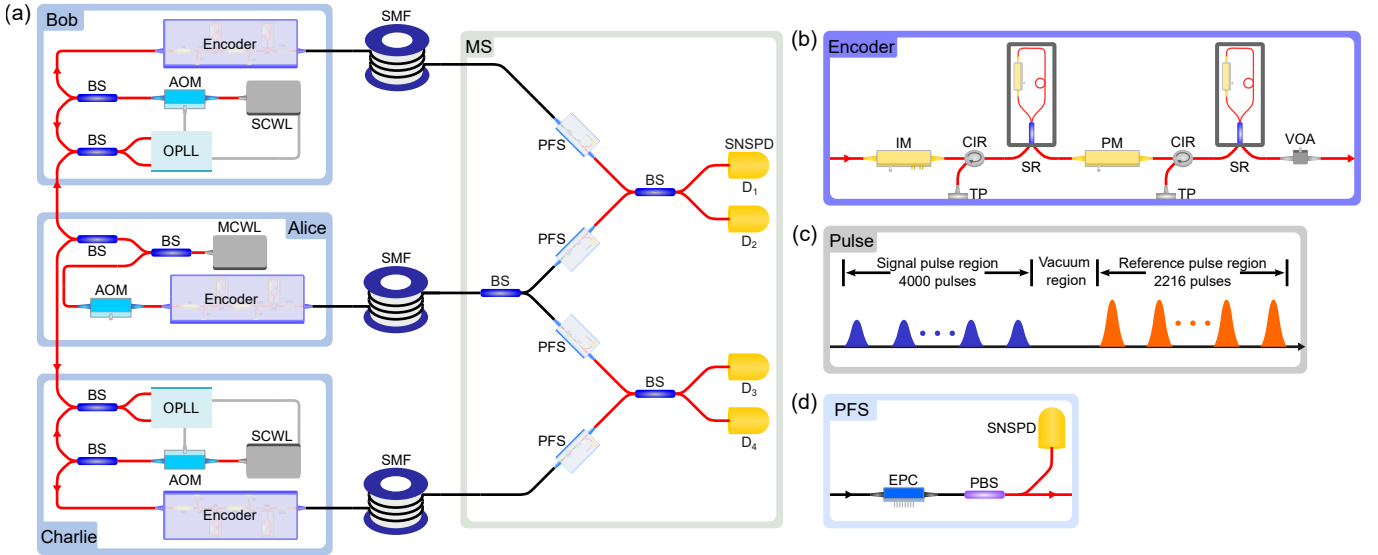


FIG. 2. Experimental setup of PM QCC protocol for three parties. (a) Layout: Three parties Alice, Bob, and Charlie are connected to the measurement site (MS) through single-mode fiber (SMF). Bob and Charlie's continuous-wave lasers (CWLs) act as slave CWLs (SCWLs), frequency locked to Alice's master CWL (MCWL) using heterodyne optical phase-locked loop (OPLL) technology with acousto-optic modulator (AOM) enhancing feedback bandwidth. Alice then uses an AOM to align the frequency of remaining MCWL beam with those of Bob and Charlie. The three parties have the same encoder for intensity and phase modulation of coherent light pulses. At the MS, Alice's coherent state is split by beam splitter (BS) into two parts, which interfere with the coherent states of Bob and Charlie in the other two BS after passing through the polarization feedback system (PFS). The interference results are then detected by four channels of superconducting nanowire single-photon detector (SNSPD). (b) Encoder: The encoder consists of an intensity modulator(IM), two Sagnac rings (SRs), two circulators (CIRs) in front of two SRs, a phase modulator (PM) between the two SRs, and a variable optical attenuator (VOA). A test port (TP) is reserved for each circulator. (c) Pulse: The encoder generates 62500 pulses per 100 μ s with 10 repeating regions excluding the pulses used for time calibration. Each repeating region consists of a reference pulse region, a vacuum region, and a signal pulse region. There are 2216 pulses in each reference pulse region and 4000 pulses in each signal pulse region. (d) PFS: The PFS is used to align the polarization of coherent light pulses. Each PFS is composed of an electric polarization controller (EPC), a polarization beamsplitter (PBS), and one channel of the detector.

pulses of 625 MHz with a pulse width of about 0.4 ns. The coherent light pulses are modulated into phase reference pulses and signal pulses by two Sagnac rings (SR) and a variable optical attenuator. The SR is a ring in which a phase modulator and a beam splitter are connected, and the phase modulator is in an asymmetric position to modulate different phases for the clockwise and counterclockwise pulses, thereby achieving the intensity modulation. The circulator in front of each SR is used to prevent the optical pulse from returning to the laser. One port of the circulator remains as the test port. The variable optical attenuator attenuates the light pulse to the single-photon level, assisting two SRs in modulating the required pulses of different intensities. The prepared signal pulses with a repetition rate of 400 MHz have three intensities corresponding to the signal state and two decoy states. The phase modulator between the two SRs is used for random phase modulation and phase coding. The signal pulses of the three parties are modulated with 16 different phases. As for the phase reference pulses, Bob and Charlie are required to modulate the pulse with three phases: 0, $\pi/2$ and $-\pi/2$, while Alice does not require phase modulation.

When the WCPs prepared by three parties arrive at the measurement site through three single-mode fiber channels, Alice's WCPs are first split into two beams to interfere with WCPs of Bob and Charlie, forming two measurement branches. The WCPs entering the two measurement branches are aligned with polarization through the polarization feedback systems, and then enter the beam splitter for interference. Finally, the interference results are detected by the four channels of superconducting nanowire single-photon detector.

Due to the imperfect frequency locking and disturbance of the fiber channel, the initial phase difference $\Delta\theta_{AB}$ ($\Delta\theta_{AC}$) between the WCPs prepared by Alice and Bob (Charlie) drift over time. The phase reference pulses are prepared and measured to track the phase drift. The statistical counts n_i^ϕ of four detector channels can be obtained every 100 μ s, where $i = 1, \dots, 4$, $\phi = 0, \pi/2, -\pi/2$ corresponding to the phase reference pulses modulated the phase of 0, $\pi/2$ or $-\pi/2$ prepared by Bob and Charlie. In this way, $\cos \Delta\theta_{AB}$, $\sin \Delta\theta_{AB}$, $\cos \Delta\theta_{AC}$, and $\sin \Delta\theta_{AC}$ can be calculated and then $\Delta\theta_{AB}$, $\Delta\theta_{AC}$ can be obtained for phase compensation every 100 μ s.

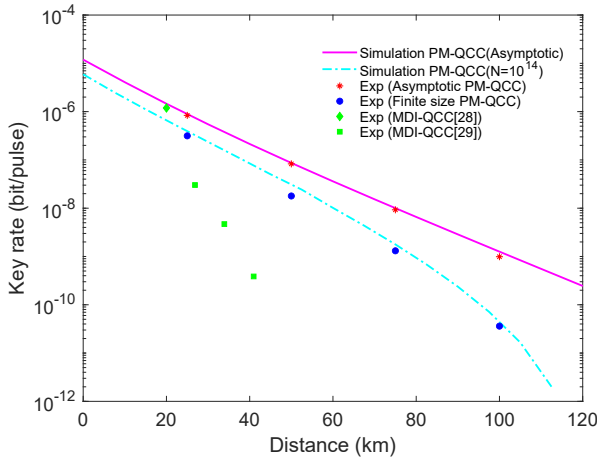


FIG. 3. Key rates for symmetric fiber channels. The magenta solid line and cyan dash-dotted line represent the simulated asymptotic key rates and the key rates with total rounds of $N = 10^{14}$ considering finite-size effects, respectively. The misalignment error $e_d = 0.03$. The red asterisks and blue solid circles represent the experimental asymptotic key rates and key rates considering finite-size effects, respectively. The green diamonds and squares represent the experimental results of Refs. [28] and [29], respectively. For comparison, attenuation used in the experiment of Ref. [29] are converted to fiber distances with the same attenuation. The error correction efficiency $f = 1.06$ [41]. The failure probability of finite-size analysis $\epsilon = 10^{-10}$.

IV. RESULTS

In the demonstration of the three-intensity PM QCC protocol, the distances for three fiber channels are represented by $\{d_A, d_B, d_C\}$, where d_A , d_B , and d_C are the distances from Alice, Bob, and Charlie to the measurement site, respectively. For the symmetric fiber channels, the key rates with total rounds of $N = 10^{14}$ considering the finite-size effects are simulated, as shown in Fig. 3. In the simulation, due to the splitting of Alice's pulse at the measurement site, the intensity of the signal state and two decoy states prepared by Alice is twice that of Bob and Charlie. The simulation results show that the maximum secure transmission distance from each party to the measurement site is over 100 km. Therefore, the three-intensity PM QCC protocol is demonstrated in the fiber configurations of $\{25, 25, 25\}$ km, $\{50, 50, 50\}$ km, $\{75, 75, 75\}$ km, and $\{100, 100, 100\}$ km, which is compatible with the intercity cryptographic applications. As shown in Table I, the total number of rounds corresponding to different fiber configurations are 2.14×10^{13} , 3.67×10^{13} , 4.66×10^{13} , and 1.28×10^{14} , and the maximum quantum bit error rates E_Z^{\max} are 3.26%, 3.30%, 3.27%, and 3.59%, respectively. The key rates considering finite-size effects and asymptotic key rates of the experiment is presented in Fig. 3. It can be observed that the gap between the key rates considering finite-size effects and the

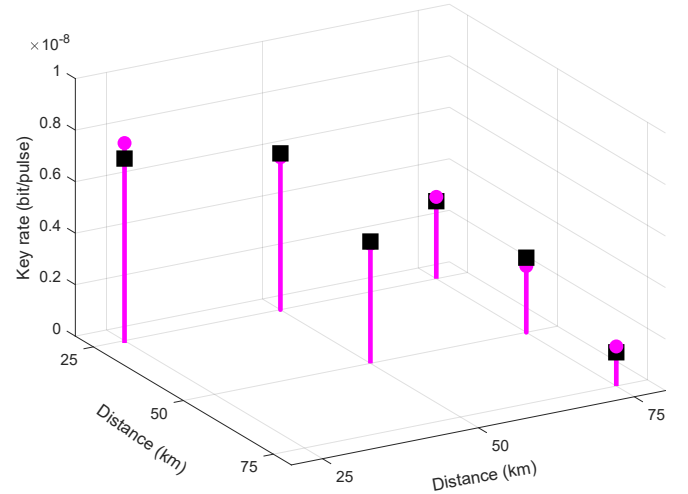


FIG. 4. Key rates for asymmetric fiber channels. The black solid squares and magenta stems represent the experimental and simulated key rates, respectively. The total number of rounds $N = 4 \times 10^{13}$ and the misalignment error $e_d = 0.03$ for simulation. The secure key rate for symmetric fiber configurations of $\{75, 75, 75\}$ km are added for comparison.

asymptotic key rate increases with distance, even though N for the channel configuration of $\{100, 100, 100\}$ km is over 10^{14} . This indicates that the implementation of PM QCC protocol is severely limited by N when the distance exceeds 100 km due to finite-size effects. More advanced and efficient protocols are needed for further enhancements [23–25]. Compared with the key rates of Refs. [28] and [29], our results have a significant improvement in the secure transmission distance and the key rate considering finite-size effects.

For the asymmetric fiber channels, the three-intensity PM QCC protocol is demonstrated in the fiber configurations of $\{75, 25, 25\}$ km, $\{75, 50, 50\}$ km, $\{75, 25, 50\}$ km, $\{75, 25, 75\}$ km, and $\{75, 50, 75\}$ km. The intensities of the signal state and the two decoy states of each party are optimized according to the channel loss while ensuring the same intensity ratio between the signal state and two decoy states. Similar to the fiber configuration of $\{75, 75, 75\}$ km, the total number of rounds of these fiber configurations is over 4×10^{13} . The key rates considering finite-size effects are shown in Fig. 4, where asymmetric fiber configurations show higher key rates compared to symmetric channels, with the $\{75, 25, 25\}$ km fiber configuration achieving a 5-fold increase over the $\{75, 75, 75\}$ km fiber configuration, eliminating the need for loss compensation in asymmetric channels. These results verify the feasibility of the three-intensity PM QCC protocol applied in real asymmetric networks.

TABLE I. Experimental parameters and results for symmetric and asymmetric channels. The detector dark count rate p_d is about 2.4×10^{-8} /pulse. The total detection efficiency η_d considering the insertion loss, the efficiency of SNSPD, the non-overlapping of the coherent pulse with the detection time window is about 60.5%. L is the length of fiber channel configuration $\{d_A, d_B, d_C\}$. R_1 is the key rate considering the finite-size effects.

L	$\{25, 25, 25\}$	$\{50, 50, 50\}$	$\{75, 75, 75\}$	$\{100, 100, 100\}$	$\{75, 50, 50\}$	$\{75, 25, 25\}$	$\{75, 50, 75\}$	$\{75, 25, 75\}$	$\{75, 25, 50\}$
E_Z^{AB}	3.26%	3.15%	3.27%	3.59%	3.27%	3.22%	3.16%	3.18%	3.31%
E_Z^{AC}	3.20%	3.30%	3.26%	3.45%	3.35%	3.27%	3.15%	3.20%	3.32%
E_X^U	13.43%	18.09%	18.12%	17.37%	17.14%	17.66%	17.01%	17.83%	17.01%
N	2.14×10^{13}	3.67×10^{13}	4.66×10^{13}	1.28×10^{14}	4.39×10^{13}	4.25×10^{13}	4.58×10^{13}	4.32×10^{13}	4.18×10^{13}
R_1	3.15×10^{-7}	1.79×10^{-8}	1.32×10^{-9}	4.20×10^{-11}	4.73×10^{-9}	6.83×10^{-9}	2.90×10^{-9}	3.00×10^{-9}	6.07×10^{-9}

V. CONCLUSION

The refined three-intensity PM QCC protocol for three parties has been applied to adapt to both symmetric and asymmetric fiber channels considering finite-size effects for experimental demonstration. In the symmetric fiber channels, the maximum secure transmission distance from each party to the measurement site reaches 100 km. In other words, the maximum fiber distance between the two parties is up to 200 km, which extends the secure transmission distance of the QCC protocol from the metropolitan area to the intercity distance. In the asymmetric fiber channels with a maximum channel distance of 75 km, higher secure key rates can be achieved using the optimized light intensities compared to the symmetric fiber channels with each channel distance of 75 km. This result verifies the feasibility of implementing PM QCC protocols for asymmetric channels in real networks without loss compensation. As our results provide a solid validation on the feasibility of implementing QCC in a real intercity star-type quantum network, we expect that this work can play a role in enriching and extending the functions and applications of current quantum networks.

ACKNOWLEDGMENTS

VI. ACKNOWLEDGMENTS

This work was supported by the Quantum Science and Technology-National Science and Technology Major Project (Grant No. 2021ZD0300702), the Anhui Initiative in Quantum Information Technologies. S. Z. acknowledges support from the Zhejiang Provincial Natural Science Foundation of China (Grant No. LQ24A050005) and the Quantum Science and Technology-National Science and Technology Major Project (Grant No. 2024ZD0302200). Y. M. acknowledges support from the National Natural Science Foundation of China (Grant No. 12104444) and the China Postdoctoral Science Foundation (Grant No. 2021M693093).

M. Z. and B.-C. L. contributed equally to this work.

Appendix A: PM QCC Protocol and Security Analysis

In this section, we first present the steps of the three-intensity PM QCC protocol. Then, we present the security foundations and prove the security of the protocol using two different methods: the entanglement-based method and the source replacement method. Next, we develop a refined decoy state method that reduces the required number of intensities for the coherent state prepared by each party, and combine the finite key analysis to estimate the upper bound of the phase error rate. Finally, we simulate the performance of the protocol.

1. Description of the PM QCC protocol

Below, we present the steps of the three-intensity PM QCC protocol for three parties.

Step.1 Preparation: As shown in Fig. 5, Alice encodes the laser pulse into the coherent state $|e^{i\varphi_A}\sqrt{\mu_A}\rangle$ with an intensity μ_A randomly chosen from $\{\mu_a, \nu_a, \omega_a\}$ with probabilities $\{p_\mu, p_\nu, p_\omega\}$, where μ_a is the intensity of signal state, ν_a and ω_a are intensities of two decoy states, $\omega_a < \nu_a < \mu_a$, and $p_\mu + p_\nu + p_\omega = 1$, and a random phase $\varphi_A = \phi_a + \pi k_a$, where $k_a \in \{0, 1\}$ is one random bit, ϕ_a is randomly chosen from $\{0, \frac{2\pi}{D}, \frac{4\pi}{D}, \dots, \frac{2\pi(D-1)}{D}\}$. Here, D is the number of phase slices. Similarly, Bob (Charlie) prepares coherent state $|e^{i\varphi_B}\sqrt{\mu_B}\rangle$ ($|e^{i\varphi_C}\sqrt{\mu_C}\rangle$) with the intensity $\mu_B \in \{\mu_b, \nu_b, \omega_b\}$ ($\mu_C \in \{\mu_c, \nu_c, \omega_c\}$) and the phase $\varphi_B = \phi_b + \pi k_b$ ($\varphi_C = \phi_c + \pi k_c$). Here, k_b (k_c) is a random bit similar to k_a , and ϕ_b (ϕ_c) is a random phase similar to ϕ_a .

Step.2 Measurement: All parties send their coherent states to the measurement site, an untrusted party Eve. An honest Eve splits each coherent pulse from Alice into two coherent pulses using a 50 : 50 beam splitter to interfere with coherent pulses from Bob and Charlie using two 50 : 50 beam splitters. The interference results of the two measurement branches formed are detected by four single-photon detectors. Eve records successful detection

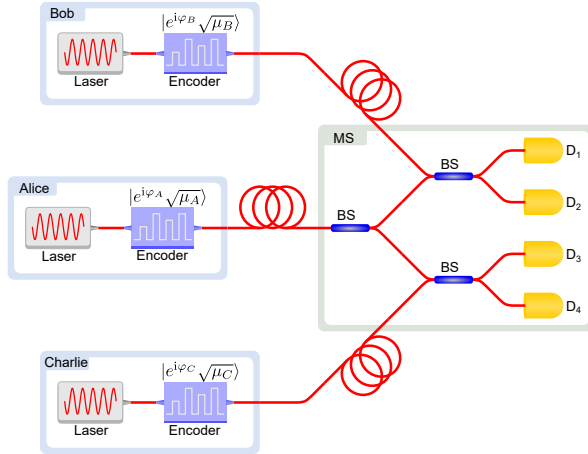


FIG. 5. PM QCC protocol for three parties. Three parties Alice, Bob, and Charlie have the same device to prepare weak coherent state. They use lasers as coherent light sources and encoders to modulate the intensity and phase of coherent light pulses, thereby preparing the required coherent states $|e^{i\varphi_A}\sqrt{\mu_A}\rangle$, $|e^{i\varphi_B}\sqrt{\mu_B}\rangle$ and $|e^{i\varphi_C}\sqrt{\mu_C}\rangle$. The coherent states prepared by the three parties are transmitted through fiber channels to the measurement site (MS). There, the coherent states prepared by Alice are split into two parts by beam splitter (BS), which interfere with the coherent states of Bob and Charlie, respectively, forming two measurement branches. The interference results of two branches are detected by four single-photon detectors (SPDs).

events. A successful detection event is defined here as a coincident click of two measurement branches, where only one detector clicks for each measurement branch.

Step.3 Announcement: Eve announces all the successful detection events, and three parties announce their random phases ϕ_a, ϕ_b, ϕ_c and intensities μ_A, μ_B, μ_C of the coherent state corresponding to each event, respectively.

Step.4 Sifting: According to announcements, Alice, Bob, and Charlie keep their random bits only when the phase-matching conditions are satisfied: $|\phi_a - \phi_b| = 0$ or π , $|\phi_a - \phi_c| = 0$ or π , and their intensities are $\{\mu_a, \mu_b, \mu_c\}$, $\{\nu_a, \nu_b, \nu_c\}$ or $\{\omega_a, \omega_b, \omega_c\}$. Then, the random bits kept by Bob and Charlie remain unchanged or are flipped, depending on the type of detection event and the announced phase result.

Step.5 Parameter estimation and key distillation: The above steps are repeated enough times to distill the raw key bits. The quantum bit error rates (QBER) E_Z^{AB} and E_Z^{AC} and the gains Q_μ, Q_ν, Q_ω can be obtained directly from the experimental results. When considering the finite-size effects, the upper and lower bounds of gains Q_μ, Q_ν, Q_ω can be estimated by the Chernoff-Hoeffding method [38]. The upper bound of the phase error rate E_X^U can be estimated using decoy-state method. Finally,

Three parties distill private key bits by performing error correction and privacy amplification on the raw key.

2. Distillation of the GHZ state

The security of multiparty quantum information protocol is contingent upon the distribution of multiparty entangled states. The PM QCC protocol is equivalent to distributing Greenberger-Horne-Zeilinger (GHZ) state

$$|\Phi^+\rangle = \frac{1}{\sqrt{2}} (|00\cdots 0\rangle + |11\cdots 1\rangle) \quad (A1)$$

directly to the participants. The secure key rate of the protocol can be obtained from the distillation efficiency of the GHZ state.

The corresponding M -qubit GHZ state basis is

$$|\Psi\rangle = \frac{1}{\sqrt{2}} (|0i_1\cdots i_{M-1}\rangle + (-1)^j |1\bar{i}_1\cdots \bar{i}_{M-1}\rangle), \quad (A2)$$

where $j(i_m) \in \{0, 1\}$ and \bar{i}_m is the logical negation of i_m . If $j = 1$ ($i_m = 1$), there is a phase (bit) error to the original GHZ state. With use of the multipartite-hashing method, the yield of distillation of the pure M -qubit GHZ state is

$$Y = 1 - \max[h(E_Z^{1,2}), h(E_Z^{1,3}), \dots, h(E_Z^{1,M})] - h(E_X), \quad (A3)$$

where $E_Z^{1,m}$ represents the bit-flip error rate of the first part and m -th part, E_X is the phase-flip error and $h(x) = -x \log_2(x) - (1-x) \log_2(1-x)$ is the binary entropy function.

3. Entanglement-based method

As shown in Fig. 6, without loss of generality, an entanglement-based PM QCC protocol for three parties that is equivalent to the prepare-and-measure PM QCC protocol is presented [19]. There is a virtual qubit at each party

$$|+\rangle = \frac{1}{\sqrt{2}} (|0\rangle + |1\rangle) \quad (A4)$$

in Fig. 6 (a). Each party prepares an entanglement state using a controlled phase gate C_π

$$C_\pi = |0\rangle\langle 0| U_0 + |1\rangle\langle 1| U_\pi \quad (A5)$$

between the virtual qubit and the coherent state, where $U_{0(\pi)}$ will attach a phase of $0(\pi)$ to the coherent state. The entanglement state prepared by the m -th participant is

$$|\Psi\rangle_m = \frac{1}{\sqrt{2}} (|0\rangle |e^{i\phi}\sqrt{\mu_m}\rangle + |1\rangle |e^{i(\phi+\pi)}\sqrt{\mu_m}\rangle), \quad (A6)$$

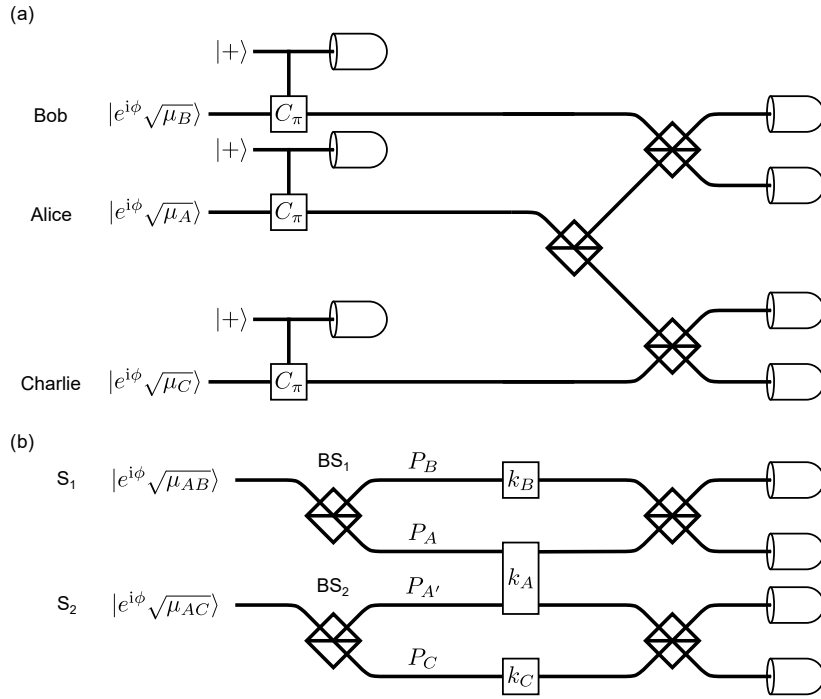


FIG. 6. (a) The entanglement-based PM QCC protocol for three parties. (b) The equivalent entanglement-based PM QCC protocol for three parties with virtual sources after beam splitting.

where the coherent state is sent to an untrusted party to perform interference measurement with the coherent

state prepared by other parties, while the virtual qubit is kept at each party.

This is equivalent to another entanglement-based version shown in Fig. 6 (b), where the initial quantum state is written as

$$|+\rangle_A |+\rangle_B |+\rangle_C \sum_{n_1=0}^{\infty} e^{-\mu_{AB}/2} \frac{\left(e^{i\phi}\sqrt{\mu_{AB}}C_1^\dagger\right)^{n_1}}{n_1!} \sum_{n_2=0}^{\infty} e^{-\mu_{AC}/2} \frac{\left(e^{i\phi}\sqrt{\mu_{AC}}C_2^\dagger\right)^{n_2}}{n_2!} |\text{vac}\rangle, \quad (\text{A7})$$

where C_i^\dagger is the creation operator of the i th virtual source, $|\text{vac}\rangle$ is the vacuum state, $\mu_{AB} = \frac{\mu_A}{2} + \mu_B$ and $\mu_{AC} = \frac{\mu_A}{2} + \mu_C$. The evolution matrix of BS_1 and BS_2 can be expressed as

$$\begin{aligned} T_{BS_1} &= \begin{bmatrix} r_1 & t_1 \\ t_1 & -r_1 \end{bmatrix}, \\ T_{BS_2} &= \begin{bmatrix} r_2 & t_2 \\ t_2 & -r_2 \end{bmatrix}, \end{aligned} \quad (\text{A8})$$

where $r_1 = \sqrt{\frac{\mu_B}{\mu_A/2 + \mu_B}}$, $t_1 = \sqrt{\frac{\mu_A/2}{\mu_A/2 + \mu_B}}$, $r_2 = \sqrt{\frac{\mu_A/2}{\mu_A/2 + \mu_C}}$, and $t_2 = \sqrt{\frac{\mu_C}{\mu_A/2 + \mu_C}}$. The quantum state takes the following form

$$\sum_{n_1, n_2=0}^{\infty} |+\rangle_A |+\rangle_B |+\rangle_C \frac{e^{-\mu_{AB}/2} (\mu_{AB})^{n_1/2}}{n_1!} \left(r_1 P_B^\dagger e^{i\phi} + t_1 P_A^\dagger e^{i\phi} \right)^{n_1} \frac{e^{-\mu_{AC}/2} (\mu_{AC})^{n_2/2}}{n_2!} \left(r_2 P_{A'}^\dagger e^{i\phi} + t_2 P_C^\dagger e^{i\phi} \right)^{n_2} |\text{vac}\rangle. \quad (\text{A9})$$

after passing through two beam splitters BS_1 and BS_2 . Here P_A^\dagger ($P_{A'}^\dagger$) and P_B^\dagger (P_C^\dagger) are the creation operators of the corresponding path mode after beam splitters BS_1 (BS_2). A C_π gate is used for bit encoding, then the quantum state

becomes

$$\frac{1}{2^{3/2}} \sum_{n_1, n_2=0}^{\infty} \frac{e^{-\mu_{\text{tot}}/2} (\mu_{AB})^{n_1/2} (\mu_{AC})^{n_2/2}}{n_1! n_2!} \left[|0\rangle |0\rangle |0\rangle \left(r_1 P_B^\dagger e^{i\phi} + t_1 P_A^\dagger e^{i\phi} \right)^{n_1} \left(r_2 P_{A'}^\dagger e^{i\phi} + t_2 P_C^\dagger e^{i\phi} \right)^{n_2} + \dots + \right. \\ \left. |1\rangle |1\rangle |1\rangle \left(-r_1 P_B^\dagger e^{i\phi} - t_1 P_A^\dagger e^{i\phi} \right)^{n_1} \left(-r_2 P_{A'}^\dagger e^{i\phi} - t_2 P_C^\dagger e^{i\phi} \right)^{n_2} \right] |\text{vac}\rangle, \quad (\text{A10})$$

where $\mu_{\text{tot}} = \mu_A + \mu_B + \mu_C$. This quantum state is equivalent to the following quantum state

$$\frac{1}{2} \sum_{n_1, n_2=0}^{\infty} \frac{e^{-\mu_{\text{tot}}/2} (\mu_{AB})^{n_1/2} (\mu_{AC})^{n_2/2}}{n_1! n_2!} \left\{ \sum_{i_A, i_C \in \{0, 1\}} \frac{1}{\sqrt{2}} \left[|0i_A i_C\rangle + (-1)^{n_1+n_2} |1\bar{i}_A \bar{i}_C\rangle \right] \right. \\ \left. \left[r_1 P_B^\dagger e^{i\phi} + (-1)^{i_A} t_1 P_A^\dagger e^{i\phi} \right]^{n_1} \left[(-1)^{i_A} r_2 P_{A'}^\dagger e^{i\phi} + (-1)^{i_C} t_2 P_C^\dagger e^{i\phi} \right]^{n_2} \right\} |\text{vac}\rangle \\ = \frac{1}{2} \sum_{n_1, n_2=0}^{\infty} \frac{e^{-\mu_{\text{tot}}/2} (\mu_{AB})^{n_1/2} (\mu_{AB})^{n_2/2}}{n_1! n_2!} \left\{ \sum_{i_A, i_C \in \{0, 1\}} \frac{1}{\sqrt{2}} \left[|0i_A i_C\rangle + (-1)^{n_1+n_2} |1\bar{i}_A \bar{i}_C\rangle \right] \right. \\ \left. \left[r_1 P_B^\dagger e^{i\phi} + (-1)^{i_A} t_1 P_A^\dagger e^{i\phi} \right]^{n_1} \left[(-1)^{i_A} r_2 P_{A'}^\dagger e^{i\phi} + (-1)^{i_C} t_2 P_C^\dagger e^{i\phi} \right]^{n_2} \right\} |\text{vac}\rangle \\ = \frac{1}{2\sqrt{2}} \sum_{i_A, i_C \in \{0, 1\}} \left\{ \sum_{n_1, n_2 \in \text{even}} \frac{e^{-\mu_{\text{tot}}/2} (\mu_{AB})^{n_1/2} (\mu_{AC})^{n_2/2}}{n_1! n_2!} \left[|0i_A i_C\rangle + |1\bar{i}_A \bar{i}_C\rangle \right] \right. \\ \left. \left[r_1 P_B^\dagger e^{i\phi} + (-1)^{i_A} t_1 P_A^\dagger e^{i\phi} \right]^{n_1} \left[(-1)^{i_A} r_2 P_{A'}^\dagger e^{i\phi} + (-1)^{i_C} t_2 P_C^\dagger e^{i\phi} \right]^{n_2} + \right. \\ \left. \sum_{n_1, n_2 \in \text{odd}} \frac{e^{-\mu_{\text{tot}}/2} (\mu_{AB})^{n_1/2} (\mu_{AC})^{n_2/2}}{n_1! n_2!} \left[|0i_A i_C\rangle + |1\bar{i}_A \bar{i}_C\rangle \right] \right. \\ \left. \left[r_1 P_B^\dagger e^{i\phi} + (-1)^{i_A} t_1 P_A^\dagger e^{i\phi} \right]^{n_1} \left[(-1)^{i_A} r_2 P_{A'}^\dagger e^{i\phi} + (-1)^{i_C} t_2 P_C^\dagger e^{i\phi} \right]^{n_2} \right\} |\text{vac}\rangle. \quad (\text{A11})$$

The quantum states held by the three participating parties are ultimately determined to be

$$\frac{1}{2} \sum_{i_A, i_C \in \{0, 1\}} \left\{ \frac{1}{\sqrt{2}} \left[|0i_A i_C\rangle + |1\bar{i}_A \bar{i}_C\rangle \right] \sqrt{p_{\text{even}}} |\text{even}\rangle + \frac{1}{\sqrt{2}} \left[|0i_A i_C\rangle - |1\bar{i}_A \bar{i}_C\rangle \right] \sqrt{p_{\text{odd}}} |\text{odd}\rangle \right\}, \quad (\text{A12})$$

where $|\text{even}\rangle$ and $|\text{odd}\rangle$ represent those states containing odd and even numbers of photons, respectively, which are given by

$$|\text{even}\rangle = \frac{1}{\sqrt{p_{\text{even}}}} \sum_{n_1, n_2 \in \text{even}} \frac{e^{-\mu_{\text{tot}}/2} (\mu_{AB})^{n_1/2} (\mu_{AC})^{n_2/2}}{n_1! n_2!} \\ \left[r_1 P_B^\dagger e^{i\phi} + (-1)^{i_A} t_1 P_A^\dagger e^{i\phi} \right]^{n_1} \left[(-1)^{i_A} r_2 P_{A'}^\dagger e^{i\phi} + (-1)^{i_C} t_2 P_C^\dagger e^{i\phi} \right]^{n_2} |\text{vac}\rangle, \\ |\text{odd}\rangle = \frac{1}{\sqrt{p_{\text{odd}}}} \sum_{n_1, n_2 \in \text{odd}} \frac{e^{-\mu_{\text{tot}}/2} (\mu_{AB})^{n_1/2} (\mu_{AC})^{n_2/2}}{n_1! n_2!} \\ \left[r_1 P_B^\dagger e^{i\phi} + (-1)^{i_A} t_1 P_A^\dagger e^{i\phi} \right]^{n_1} \left[(-1)^{i_A} r_2 P_{A'}^\dagger e^{i\phi} + (-1)^{i_C} t_2 P_C^\dagger e^{i\phi} \right]^{n_2} |\text{vac}\rangle, \quad (\text{A13})$$

and $\sqrt{p_{\text{even}}}$ and $\sqrt{p_{\text{odd}}}$ are normalized coefficients of pure states $|\text{even}\rangle$ and $|\text{odd}\rangle$, which are given by

$$p_{\text{even}} = \sum_{n_1, n_2 \in \text{even}} \frac{e^{-\mu_{\text{tot}}/2} (\mu_{AB})^{n_1/2} (\mu_{AC})^{n_2/2}}{n_1! n_2!} = e^{-\mu_{\text{tot}}} \cosh(\mu_{\text{tot}}), \\ p_{\text{odd}} = \sum_{n_1, n_2 \in \text{odd}} \frac{e^{-\mu_{\text{tot}}/2} (\mu_{AB})^{n_1/2} (\mu_{AC})^{n_2/2}}{n_1! n_2!} = e^{-\mu_{\text{tot}}} \sinh(\mu_{\text{tot}}). \quad (\text{A14})$$

Thus, according to the description in Sec. A 2, the phase error rate E_X can be estimated by

$$E_X = p_{\text{odd}} \frac{Y_{\text{odd}}}{Q_\mu}, \quad (\text{A15})$$

where Y_{odd} is the overall yield for odd-number components, and Q_μ is the overall gain of signal state.

4. Source replacement method

As shown in Fig. 7, we employ the source replacement method [39] to make the security proof of the PM QCC

protocol more intuitive. A protocol equivalent to PM QCC can be represented as a quantum gate encoding circuit. The initial state of circuit can be expressed as

$$|+_d\rangle_{A_0} |+\rangle_{A_1} |\alpha\rangle_A |+_d\rangle_{B_0} |+\rangle_{B_1} |\beta\rangle_B |+_d\rangle_{C_0} |+\rangle_{C_1} |\gamma\rangle_C, \quad (\text{A16})$$

where $|+\rangle = \frac{1}{\sqrt{2}}(|0\rangle + |1\rangle)$, $|+_d\rangle$ is the eigen state of Pauli X operator in d-dimension and $|\alpha\rangle$, $|\beta\rangle$, and $|\gamma\rangle$ are coherent state. The Z-basis measurement results at $|+\rangle$ and $|+_d\rangle$ control the key bit encoding using $C - \theta_a$, $C - \theta_b$, and $C - \theta_c$ gates and the random phase encoding using $C - \theta_j$ gate, respectively.

Once the initial quantum state is operated by these C-phase gates, the auxiliary systems of Alice, Bob, and Charlie are entangled with the optical modes sent for interference measurement. The initial quantum state is transformed into

$$\left(\frac{1}{2d} \right)^{\frac{3}{2}} \left[\sum_{j_a=0}^{d-1} |j_a\rangle_{A_0} \left(|0\rangle_{A_1} \left| e^{2\pi i j_a/d} \alpha \right\rangle_A + |1\rangle_{A_1} \left| -e^{2\pi i j_a/d} \alpha \right\rangle_A \right) \right. \\ \left. \sum_{j_b=0}^{d-1} |j_b\rangle_{B_0} \left(|0\rangle_{B_1} \left| e^{2\pi i j_b/d} \beta \right\rangle_B + |1\rangle_{B_1} \left| -e^{2\pi i j_b/d} \beta \right\rangle_B \right) \right. \\ \left. \sum_{j_c=0}^{d-1} |j_c\rangle_{C_0} \left(|0\rangle_{C_1} \left| e^{2\pi i j_c/d} \gamma \right\rangle_C + |1\rangle_{C_1} \left| -e^{2\pi i j_c/d} \gamma \right\rangle_C \right) \right]. \quad (\text{A17})$$

Following the operation of two CNOT gates, the quantum state undergoes unitary evolution into

$$\left(\frac{1}{2d} \right)^{\frac{3}{2}} \left[\sum_{j_a=0}^{d-1} |j_a\rangle_{A_0} \left(|0\rangle_{A_1} \left| e^{2\pi i j_a/d} \alpha \right\rangle_A + |1\rangle_{A_1} \left| -e^{2\pi i j_a/d} \alpha \right\rangle_A \right) \right. \\ \left. \sum_{j_b=0}^{d-1} |j_b - j_a\rangle_{B_0} \left(|0\rangle_{B_1} \left| e^{2\pi i j_b/d} \beta \right\rangle_B + |1\rangle_{B_1} \left| -e^{2\pi i j_b/d} \beta \right\rangle_B \right) \right. \\ \left. \sum_{j_c=0}^{d-1} |j_c - j_a\rangle_{C_0} \left(|0\rangle_{C_1} \left| e^{2\pi i j_c/d} \gamma \right\rangle_C + |1\rangle_{C_1} \left| -e^{2\pi i j_c/d} \gamma \right\rangle_C \right) \right] \\ = \left(\frac{1}{2d} \right)^{\frac{3}{2}} \sum_{j_1=0}^{d-1} \sum_{j_2=0}^{d-1} \sum_{j_a=0}^{d-1} |j_a\rangle_{A_0} \left(|0\rangle_{A_1} \left| e^{2\pi i j_a/d} \alpha \right\rangle_A + |1\rangle_{A_1} \left| -e^{2\pi i j_a/d} \alpha \right\rangle_A \right) \\ |j_1\rangle_{B_0} \left(|0\rangle_{B_1} \left| e^{2\pi i (j_1+j_a)/d} \beta \right\rangle_B + |1\rangle_{B_1} \left| -e^{2\pi i (j_1+j_a)/d} \beta \right\rangle_B \right) \\ |j_2\rangle_{C_0} \left(|0\rangle_{C_1} \left| e^{2\pi i (j_2+j_a)/d} \gamma \right\rangle_C + |1\rangle_{C_1} \left| -e^{2\pi i (j_2+j_a)/d} \gamma \right\rangle_C \right), \quad (\text{A18})$$

where $j_1 = j_b - j_a$ and $j_2 = j_c - j_a$. Acting a quantum inverse Fourier transform gate F^\dagger on A_0 results in

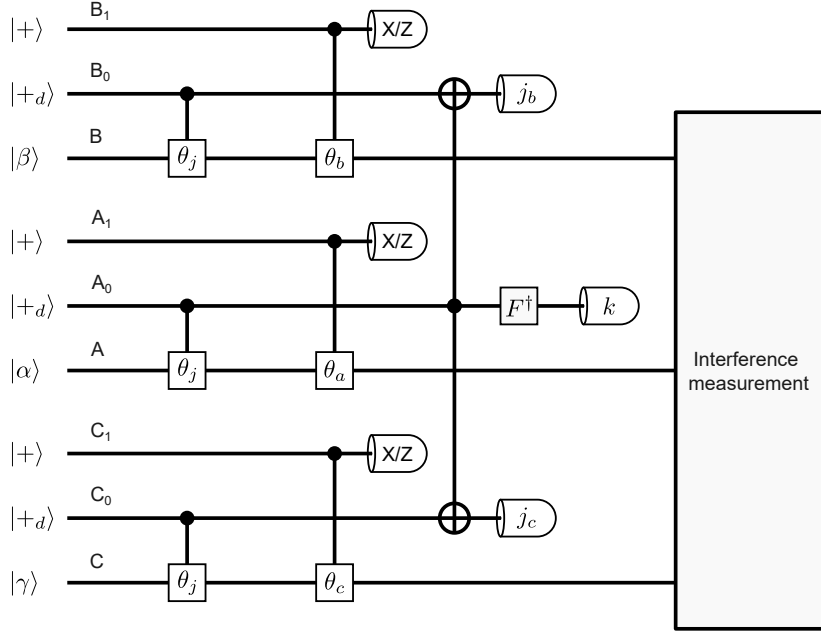


FIG. 7. Encoding circuit of source-replaced scheme. The auxiliary systems A_0 , A_1 , B_0 , B_1 , C_0 and C_1 are used to encode the random phases and key bits. Subsequent to the encoding of coherent states, the auxiliary systems undergo gate operations and measurements, which can be utilized to determine the phase and bit error rates of the entangled system. The gate operations involved in this process include a quantum inverse Fourier transform, denoted by F^\dagger , applied to the auxiliary system of Alice, together with two high-dimensional CNOT operations.

$$\begin{aligned}
& \left(\frac{1}{2}\right)^{\frac{3}{2}} \left(\frac{1}{d}\right)^2 \sum_{j_1=0}^{d-1} \sum_{j_2=0}^{d-1} \sum_{j_a=0}^{d-1} \sum_{k=0}^{d-1} e^{-2\pi i k j_a / d} \\
& |k\rangle_{A_0} \left(|0\rangle_{A_1} \left| -e^{2\pi i j_a / d} \alpha \right\rangle_A + |1\rangle_{A_1} \left| -e^{2\pi i j_a / d} \alpha \right\rangle_A \right) \\
& |j_1\rangle_{B_0} \left(|0\rangle_{B_1} \left| e^{2\pi i (j_1 + j_a) / d} \beta \right\rangle_B + |1\rangle_{B_1} \left| -e^{2\pi i (j_1 + j_a) / d} \beta \right\rangle_B \right) \\
& |j_2\rangle_{C_0} \left(|0\rangle_{C_1} \left| e^{2\pi i (j_2 + j_a) / d} \gamma \right\rangle_C + |1\rangle_{C_1} \left| -e^{2\pi i (j_2 + j_a) / d} \gamma \right\rangle_C \right), \tag{A19}
\end{aligned}$$

where

$$F^\dagger = \frac{1}{\sqrt{d}} \sum_{j=0}^{d-1} \sum_{k=0}^{d-1} e^{-2\pi i j k / d} |k\rangle \langle j|. \tag{A20}$$

Subsequent to the implementation of projective measurements on the auxiliary systems A_0 , B_0 , and C_0 in their respective basis, the final system evolves into

$$\begin{aligned}
& \sum_{j_a=0}^{d-1} e^{-2\pi i k j_a / d} \left(|0\rangle_{A_1} \left| e^{2\pi i j_a / d} \alpha \right\rangle_A + |1\rangle_{A_1} \left| -e^{2\pi i j_a / d} \alpha \right\rangle_A \right) \\
& \left(|0\rangle_{B_1} \left| e^{2\pi i j_a / d} \beta' \right\rangle_B + |1\rangle_{B_1} \left| -e^{2\pi i j_a / d} \beta' \right\rangle_B \right) \left(|0\rangle_{C_1} \left| e^{2\pi i j_a / d} \gamma' \right\rangle_C + |1\rangle_{C_1} \left| -e^{2\pi i j_a / d} \gamma' \right\rangle_C \right) \\
& = e^{-(|\alpha|^2 + |\beta'|^2 + |\gamma'|^2)/2} \sum_{j_a=0}^{d-1} \sum_{n=0}^{\infty} \sum_{m=0}^{\infty} \sum_{l=0}^{\infty} e^{2\pi i (n+m+l-k) j_a / d} \\
& [[0\rangle + (-1)^n |1\rangle]_{A_1} [[0\rangle + (-1)^m |1\rangle]_{B_1} [[0\rangle + (-1)^l |1\rangle]_{C_1} \frac{\alpha^n \beta'^m \gamma'^l}{\sqrt{n! m! l!}} |nml\rangle_{ABC}. \tag{A21}
\end{aligned}$$

Here, $e^{2\pi i j_b/d}\beta$ is denoted as β' and $e^{2\pi i j_c/d}\gamma$ is denoted as γ' for clarity. After performing the interference measurement on coherent state, if $n+m+l$ is even (odd), the state shared by Alice, Bob and Charlie is the linear combination of $\frac{i}{\sqrt{2}}(|0ij\rangle + |1\bar{i}\bar{j}\rangle)$ ($\frac{1}{\sqrt{2}}(|0ij\rangle - |1\bar{i}\bar{j}\rangle)$). The key bits can be obtained by performing Z-basis measurements on the auxiliary systems A_1 , B_1 , and C_1 , whose phase error rate can be obtained by performing X-basis measurements on these auxiliary systems. According to the analysis of Sec. A 2, the phase error rate expressed as Eq. (A15) can be obtained.

5. Decoy-state method

The phase errors rate E_X in Eq. (A15) can be rewritten as

$$\begin{aligned} E_X &= \sum_{k \in \text{odd}} P_\mu(k) \frac{Y_k}{Q_\mu} \\ &= 1 - \sum_{k \in \text{even}} P_\mu(k) \frac{Y_k}{Q_\mu} \\ &\leq E_X^U = 1 - P_\mu(2) \frac{Y_2^L}{Q_\mu}, \end{aligned} \quad (\text{A22})$$

where $P_\mu(k)$ is the probability that all parties emit k photons, following a Poisson distribution with total intensity μ_{tot} as the parameter. Y_2^L is the lower bound of the yield of two photons, which can be estimated by decoy-state method with the intensity set $\{\mu, \nu, \omega, 0\}$. Define

$$\begin{aligned} \mu_{\text{tot}} &= \mu_a + \mu_b + \mu_c, \\ \nu_{\text{tot}} &= \nu_a + \mu_b + \nu_c, \\ \omega_{\text{tot}} &= \omega_a + \omega_b + \omega_c, \\ \mu_{\text{tot}} &> \nu_{\text{tot}} > \omega_{\text{tot}}. \end{aligned} \quad (\text{A23})$$

Here $\mu_a : \nu_a : \omega_a = \mu_b : \nu_b : \omega_b = \mu_c : \nu_c : \omega_c$ is assumed. Then

$$\begin{aligned} e^{\mu_{\text{tot}}} Q_\mu &= Y_0 + 2\mu_{\text{tot}} Y_1 + \frac{\mu_{\text{tot}}^2}{2} Y_2 + \frac{\mu_{\text{tot}}^3}{6} Y_3 + \dots, \\ e^{\nu_{\text{tot}}} Q_\nu &= Y_0 + 2\nu_{\text{tot}} Y_1 + \frac{\nu_{\text{tot}}^2}{2} Y_2 + \frac{\nu_{\text{tot}}^3}{6} Y_3 + \dots, \\ e^{\omega_{\text{tot}}} Q_\omega &= Y_0 + 2\omega_{\text{tot}} Y_1 + \frac{\omega_{\text{tot}}^2}{2} Y_2 + \frac{\omega_{\text{tot}}^3}{6} Y_3 + \dots, \\ Q_0 &= Y_0. \end{aligned} \quad (\text{A24})$$

Using the Gaussian-elimination method, we have

$$Y_2 \geq \frac{2}{G} (G_\nu Q_\nu + G_0 Q_0 - G_\mu Q_\mu - G_\omega Q_\omega), \quad (\text{A25})$$

where

$$\begin{aligned} G &= (\mu_{\text{tot}} - \nu_{\text{tot}})(\nu_{\text{tot}} - \omega_{\text{tot}}) \mu_{\text{tot}} \nu_{\text{tot}}^2 \omega_{\text{tot}} (\mu_{\text{tot}} - \omega_{\text{tot}}) > 0, \\ G_\nu &= \mu_{\text{tot}} \nu_{\text{tot}} \omega_{\text{tot}} e^{\nu_{\text{tot}}} (\mu_{\text{tot}}^2 - \omega_{\text{tot}}^2) > 0, \\ G_0 &= (\mu_{\text{tot}} - \nu_{\text{tot}})(\nu_{\text{tot}} - \omega_{\text{tot}}) \nu_{\text{tot}} \\ &\quad [\mu_{\text{tot}}(\mu_{\text{tot}} + \nu_{\text{tot}}) - \omega_{\text{tot}}(\nu_{\text{tot}} + \omega_{\text{tot}})] > 0, \\ G_\mu &= (\nu_{\text{tot}}^2 - \omega_{\text{tot}}^2) \nu_{\text{tot}}^2 \omega_{\text{tot}} e^{\mu_{\text{tot}}} > 0, \\ G_\omega &= (\mu_{\text{tot}}^2 - \nu_{\text{tot}}^2) \mu_{\text{tot}} \nu_{\text{tot}}^2 e^{\omega_{\text{tot}}} > 0. \end{aligned} \quad (\text{A26})$$

Thus $Q_0 G_0 \geq 0$ and

$$Y_2 \geq Y_2^L = \frac{2}{G} (G_\nu Q_\nu - G_\mu Q_\mu - G_\omega Q_\omega). \quad (\text{A27})$$

Based on the yield of distillation of the pure 3-qubit GHZ state, the key rate of PM QCC protocol can be expressed as

$$R = \left(\frac{2}{D}\right)^2 Q_\mu [1 - fh(E_Z^{\max}) - h(E_X^U)], \quad (\text{A28})$$

where $(2/D)^2$ is the prefactor induced by phase post-selection.

6. Finite-size analysis

Given an observed quantity χ , follow the Chernoff-Hoeffding method in Ref. [38], the upper bound and lower bound of the underlying expectation value are given by

$$\begin{aligned} \mathbb{E}^L(\chi) &= \frac{\chi}{1 + \delta^L}, \\ \mathbb{E}^U(\chi) &= \frac{\chi}{1 - \delta^U}, \end{aligned} \quad (\text{A29})$$

where $\delta^{L(U)}$ is the solution of

$$\begin{aligned} \left[\frac{e^{\delta^L}}{(1 + \delta^L)^{1 + \delta^L}} \right]^{\chi/(1 + \delta^L)} &= \frac{1}{2} \epsilon, \\ \left[\frac{e^{-\delta^U}}{(1 - \delta^U)^{1 - \delta^U}} \right]^{\chi/(1 - \delta^U)} &= \frac{1}{2} \epsilon. \end{aligned} \quad (\text{A30})$$

The ϵ is failure probability of the estimation $\mathbb{E}(\chi) \in [\mathbb{E}^L(\chi), \mathbb{E}^U(\chi)]$. When finite-size effects are considered, the lower bound of the yield of two-photon state is given by

$$Y_2^L = \frac{2}{G} (G_\nu Q_\nu^L - G_\mu Q_\mu^U - G_\omega Q_\omega^U), \quad (\text{A31})$$

where Q_μ^U and Q_ω^U are the upper bounds of Q_μ and Q_ω , respectively, and Q_ν^L is the lower bound of Q_ν .

7. Simulation method and result

Firstly, we obtain the click probability in the PM QCC protocol, and then calculate the gain under the given information of the sender and the channel. The intensity of coherent state prepared by Alice, Bob and Charlie are denoted as $\mu_A \in \{\mu_a, \nu_a, \omega_a\}$, $\mu_B \in \{\mu_b, \nu_b, \omega_b\}$ and $\mu_C \in \{\mu_c, \nu_c, \omega_c\}$, respectively. The transmittance from Alice, Bob, Charlie to the measurement site are denoted as η_A , η_B and η_C . The total detection efficiency of measurement site is η_d . The click probabilities of two measurement branches for each coherent pulse are given by

$$\begin{aligned} p_{\mu_A, \mu_B}^{\text{click}} &= 1 - e^{-\eta_A \eta_d \mu_A / 2 - \eta_B \eta_d \mu_B} + \\ &\quad 2p_d e^{-\eta_A \eta_d \mu_A / 2 - \eta_B \eta_d \mu_B}, \\ p_{\mu_A, \mu_C}^{\text{click}} &= 1 - e^{-\eta_A \eta_d \mu_A / 2 - \eta_C \eta_d \mu_C} + \\ &\quad 2p_d e^{-\eta_A \eta_d \mu_A / 2 - \eta_C \eta_d \mu_C}, \end{aligned} \quad (\text{A32})$$

where p_d represents the dark count rate of the single-photon detector. The gain can be written as

$$Q_{\mu_A, \mu_B, \mu_C} = p_{\mu_A, \mu_B}^{\text{click}} p_{\mu_A, \mu_C}^{\text{click}}. \quad (\text{A33})$$

The sending probabilities of signal state and two decoy states for each party are denoted as p_μ , p_ν , and p_ω , respectively. The total number of rounds is denoted as N . Thus, the number of rounds in which Alice, Bob, and Charlie simultaneously send signal and two decoy states are given by

$$\begin{aligned} N_\mu &= N p_\mu^3, \\ N_\nu &= N p_\nu^3, \\ N_\omega &= N p_\omega^3. \end{aligned} \quad (\text{A34})$$

The effective clicks for simultaneously sending signal and two decoy states are given by

$$\begin{aligned} M_\mu &= N_\mu Q_{\mu_a, \mu_b, \mu_c} = N_\mu Q_\mu, \\ M_\nu &= N_\nu Q_{\nu_a, \nu_b, \nu_c} = N_\nu Q_\nu, \\ M_\omega &= N_\omega Q_{\omega_a, \omega_b, \omega_c} = N_\omega Q_\omega. \end{aligned} \quad (\text{A35})$$

Based on the finite-key analysis method in Sec. A 6, The statistical upper and lower bounds of the effective

clicks can be calculated by the Chernoff bound method. Then the upper and lower bounds of the gain for each state can be obtained. By substituting it into Eq. (A31), the lower bound of the two-photon yield can be derived.

The upper bound of the phase error can be written as

$$E_X^U = 1 - e^{-\mu_{\text{tot}}} \frac{\mu_{\text{tot}}^2}{2Y_2^L Q_\mu^L}. \quad (\text{A36})$$

The quantum bit error rate can be expressed by

$$E_Z^{\text{max}} = \max\{e^{AB}, e^{AC}\} + e_d, \quad (\text{A37})$$

where e_d is the misalignment error, e^{AB} and e^{AC} are intrinsic errors of two measurement branch caused by dark counts and the discretization of the phase slice, which are given by

$$\begin{aligned} e^{AB} &= \frac{1}{p_{\mu_a, \mu_b}^{\text{click}}} [p_d + (\eta_A \eta_d \mu_a / 2 + \eta_B \eta_d \mu_b) e_\delta] \\ &\quad e^{-\eta_A \eta_d \mu_a / 2 - \eta_B \eta_d \mu_b}, \\ e^{AC} &= \frac{1}{p_{\mu_a, \mu_c}^{\text{click}}} [p_d + (\eta_A \eta_d \mu_a / 2 + \eta_C \eta_d \mu_c) e_\delta] \\ &\quad e^{-\eta_A \eta_d \mu_a / 2 - \eta_C \eta_d \mu_c}, \\ e_\delta &= \frac{\pi}{D} - \left(\frac{D}{\pi}\right)^2 \left(\sin \frac{\pi}{D}\right)^3. \end{aligned} \quad (\text{A38})$$

Finally, the key rates can be obtained by substituting Eq. (A36) and Eq. (A37) into Eq. (A28). The simulation results for symmetric and asymmetric channels are given in Fig. 8. In Fig. 8 (a), the key rates in symmetric fiber channels are simulated under the number of rounds N of 10^{13} , 10^{14} , and 10^{15} , respectively. In Fig. 8 (b), the key rates in asymmetric fiber channels are simulated where the distance from Alice to the measurement site is fixed at 75 km, while the distances from Bob and Charlie to the measurement site are vary from 0 to 75 km, respectively.

Appendix B: Experimental parameters and results

In this section, we provide more detailed experimental parameters and results for symmetric and asymmetric channels compared to the main text, as shown in Table II.

[1] H. J. Kimble, *Nature* **453**, 1023 (2008).
[2] S. Wehner, D. Elkouss, and R. Hanson, *Science* **362**, eaam9288 (2018).
[3] J. Nokkala, J. Piilo, and G. Bianconi, *Journal of Physics A: Mathematical and Theoretical* **57**, 233001 (2024).
[4] V. Scarani, H. Bechmann-Pasquinucci, N. J. Cerf, M. Dušek, N. Lütkenhaus, and M. Peev, *Rev. Mod. Phys.* **81**, 1301 (2009).
[5] F. Xu, X. Ma, Q. Zhang, H.-K. Lo, and J.-W. Pan, *Rev. Mod. Phys.* **92**, 025002 (2020).
[6] M. Peev, C. Pacher, R. Alléaume, C. Barreiro, J. Bouda, W. Boxleitner, T. Debuisschert, E. Diamanti, M. Dianati, J. F. Dynes, *et al.*, *New Journal of Physics* **11**, 075001 (2009).
[7] T.-Y. Chen, J. Wang, H. Liang, W.-Y. Liu, Y. Liu, X. Jiang, Y. Wang, X. Wan, W.-Q. Cai, L. Ju, *et al.*, *Opt. Express* **18**, 27217 (2010).
[8] M. Sasaki, M. Fujiwara, H. Ishizuka, W. Klaus, K. Wakui, M. Takeoka, S. Miki, T. Yamashita, Z. Wang, A. Tanaka, *et al.*, *Opt. Express* **19**, 10387 (2011).

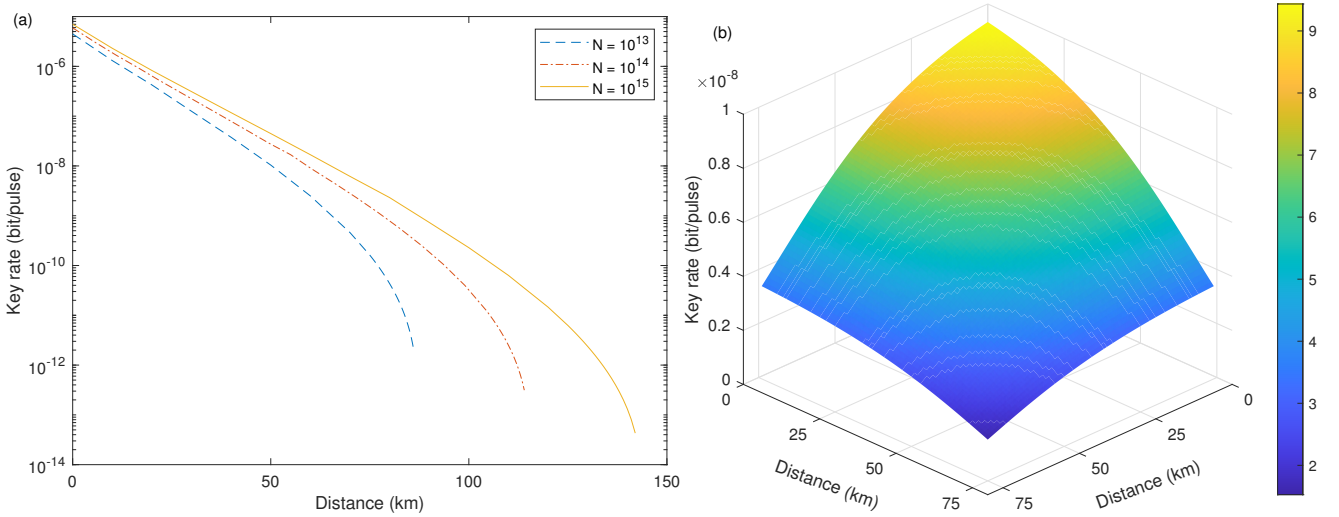


FIG. 8. Simulation of key rates. The error correction efficiency $f = 1.06$. The failure probability of bound for finite-size analysis $\epsilon = 10^{-10}$. The number of phase slices $D = 16$. The attenuation coefficient of optical fiber $\alpha = 0.175$ dB/km. The detector dark count rate $p_d = 2.4 \times 10^{-8}$ /pulse. The total detection efficiency $\eta_d = 0.6$. The intensity and sending probability of the coherent states prepared by each party are optimized to achieve the highest key rate. (a) Simulated key rates in symmetric fiber channels. The number of rounds N corresponding to the dashed line, solid line, and dash-dotted line are 10^{13} , 10^{14} , and 10^{15} , respectively. (b) Simulated key rates in asymmetric fiber channels. The distance from Alice to the measurement site is fixed at 75 km, while the distances from Bob and Charlie to the measurement site are represented by the X-axis and Y-axis, respectively. Here $N = 4 \times 10^{13}$.

TABLE II. Experimental parameters and results for symmetric and asymmetric channels. N_μ (N_ν , N_ω) is the number of rounds in which Alice, Bob, and Charlie simultaneously send signal (decoy) states with intensities μ_a (ν_a, ω_a), μ_b (ν_b, ω_b) and μ_c (ν_c, ω_c). The probabilities of each party corresponding to the sending signal state and two decoy states are represented as p_μ , p_ν , and p_ω , respectively. The transmittance from Alice (Bob, Charlie) to the measurement site is denoted as η_A (η_B , η_C). Note that η_A contains the loss of the BS used for the splitting of Alice's coherent pulse at the measurement site. M_μ (M_ν , M_ω) is the effective clicks for simultaneously sending signal (decoy) states with intensities μ_a (ν_a, ω_a), μ_b (ν_b, ω_b) and μ_c (ν_c, ω_c). K is the raw key length. R_1 is the key rate considering the finite-size effects. R_2 is the asymptotic key rate.

L	{25, 25, 25}	{50, 50, 50}	{75, 75, 75}	{100, 100, 100}	{75, 50, 50}	{75, 25, 25}	{75, 50, 75}	{75, 25, 75}	{75, 25, 50}
μ_a	7.39×10^{-2}	7.73×10^{-2}	7.21×10^{-2}	6.14×10^{-2}	1.05×10^{-1}	1.27×10^{-1}	8.45×10^{-2}	9.13×10^{-2}	1.17×10^{-1}
μ_b	3.75×10^{-2}	3.54×10^{-2}	3.57×10^{-2}	3.15×10^{-2}	1.85×10^{-2}	8.99×10^{-3}	1.50×10^{-2}	6.60×10^{-3}	8.18×10^{-3}
μ_c	3.58×10^{-2}	3.55×10^{-2}	3.42×10^{-2}	2.92×10^{-2}	1.90×10^{-2}	8.67×10^{-3}	4.14×10^{-2}	4.52×10^{-2}	2.02×10^{-2}
ν_a	3.88×10^{-2}	4.19×10^{-2}	3.95×10^{-2}	3.23×10^{-2}	5.74×10^{-2}	7.00×10^{-2}	4.63×10^{-2}	4.97×10^{-2}	6.40×10^{-2}
ν_b	1.95×10^{-2}	1.92×10^{-2}	1.96×10^{-2}	1.67×10^{-2}	1.01×10^{-2}	4.95×10^{-3}	8.31×10^{-3}	3.62×10^{-3}	4.47×10^{-3}
ν_c	1.87×10^{-2}	1.93×10^{-2}	1.87×10^{-2}	1.55×10^{-2}	1.04×10^{-2}	4.78×10^{-3}	2.30×10^{-2}	2.47×10^{-2}	1.10×10^{-2}
ω_a	1.88×10^{-3}	2.83×10^{-3}	2.88×10^{-3}	2.73×10^{-3}	3.96×10^{-3}	4.60×10^{-3}	3.39×10^{-3}	3.47×10^{-3}	4.31×10^{-3}
ω_b	9.79×10^{-4}	1.29×10^{-3}	1.46×10^{-3}	1.39×10^{-3}	7.18×10^{-4}	3.18×10^{-4}	5.98×10^{-4}	2.54×10^{-4}	3.03×10^{-4}
ω_c	9.53×10^{-4}	1.25×10^{-3}	1.42×10^{-3}	1.29×10^{-3}	7.16×10^{-4}	3.14×10^{-4}	1.61×10^{-3}	1.74×10^{-3}	7.48×10^{-4}
N_μ	1.10×10^{13}	1.30×10^{13}	9.80×10^{12}	7.52×10^{12}	1.25×10^{13}	1.37×10^{13}	1.12×10^{13}	1.12×10^{13}	1.26×10^{13}
N_ν	2.46×10^{10}	1.12×10^{11}	3.70×10^{11}	3.12×10^{12}	2.20×10^{11}	1.70×10^{11}	2.90×10^{11}	2.69×10^{11}	1.89×10^{11}
N_ω	1.98×10^{10}	1.19×10^{11}	4.13×10^{11}	4.18×10^{12}	2.42×10^{11}	2.03×10^{11}	3.33×10^{11}	3.16×10^{11}	1.95×10^{11}
p_μ	0.8003	0.7079	0.5950	0.3916	0.6572	0.6850	0.6258	0.6370	0.6706
p_ν	0.1030	0.1442	0.1977	0.2897	0.1685	0.1550	0.1833	0.1780	0.1621
p_ω	0.0967	0.1479	0.2073	0.3187	0.1743	0.1600	0.1909	0.1850	0.1673
η_A	0.1687	0.0635	0.0241	0.0090	0.0241	0.0241	0.0241	0.0241	0.0241
η_B	0.3381	0.1409	0.0475	0.0171	0.1409	0.3381	0.1409	0.3381	0.3381
η_C	0.3420	0.1380	0.0499	0.0194	0.1380	0.3420	0.0499	0.0499	0.1380
M_μ	2040135966	437817496	40466521	3557353	115848639	173509703	66660580	77230873	135241099
M_ν	1272088	1102148	458942	410061	609615	659095	526434	554995	604702
M_ω	2482	5401	2790	3915	3306	3365	3045	3258	2872
K	31944815	6832717	631442	55251	1810617	2710929	1041251	1209357	2116983
R_1	3.15×10^{-7}	1.79×10^{-8}	1.32×10^{-9}	4.20×10^{-11}	4.73×10^{-9}	6.83×10^{-9}	2.90×10^{-9}	3.00×10^{-9}	6.07×10^{-9}
R_2	8.37×10^{-7}	8.28×10^{-8}	9.26×10^{-9}	9.89×10^{-10}	3.01×10^{-8}	3.82×10^{-8}	2.13×10^{-8}	2.15×10^{-8}	3.57×10^{-8}

[9] Y.-L. Tang, H.-L. Yin, Q. Zhao, H. Liu, X.-X. Sun, M.-Q. Huang, W.-J. Zhang, S.-J. Chen, L. Zhang, L.-X. You, *et al.*, [Phys. Rev. X](#) **6**, 011024 (2016).

[10] S. K. Joshi, D. Aktas, S. Wengerowsky, M. Lončarić, S. P. Neumann, B. Liu, T. Scheidl, G. C. Lorenzo, Željko Samec, L. Kling, *et al.*, [Science Advances](#) **6**, eaba0959 (2020).

[11] Y.-A. Chen, Q. Zhang, T.-Y. Chen, W.-Q. Cai, S.-K. Liao, J. Zhang, K. Chen, J. Yin, J.-G. Ren, Z. Chen, *et al.*, [Nature](#) **589**, 214 (2021).

[12] X. Zhong, W. Wang, R. Mandil, H.-K. Lo, and L. Qian, [Phys. Rev. Appl.](#) **17**, 014025 (2022).

[13] K. Chen and H.-K. Lo, [Quantum Info. Comput.](#) **7**, 689–715 (2007).

[14] Y. Fu, H.-L. Yin, T.-Y. Chen, and Z.-B. Chen, [Phys. Rev. Lett.](#) **114**, 090501 (2015).

[15] M. Epping, H. Kampermann, C. macchiavello, and D. Bruß, [New Journal of Physics](#) **19**, 093012 (2017).

[16] F. Grasselli, H. Kampermann, and D. Bruß, [New Journal of Physics](#) **20**, 113014 (2018).

[17] F. Grasselli, H. Kampermann, and D. Bruß, [New Journal of Physics](#) **21**, 123002 (2019).

[18] G. Murta, F. Grasselli, H. Kampermann, and D. Bruß, [Advanced Quantum Technologies](#) **3**, 2000025 (2020).

[19] S. Zhao, P. Zeng, W.-F. Cao, X.-Y. Xu, Y.-Z. Zhen, X. Ma, L. Li, N.-L. Liu, and K. Chen, [Phys. Rev. Appl.](#) **14**, 024010 (2020).

[20] X.-Y. Cao, Y.-S. Lu, Z. Li, J. Gu, H.-L. Yin, and Z.-B. Chen, [IEEE Access](#) **9**, 128870 (2021).

[21] X.-Y. Cao, J. Gu, Y.-S. Lu, H.-L. Yin, and Z.-B. Chen, [New Journal of Physics](#) **23**, 043002 (2021).

[22] X. Hua, M. Hu, and B. Guo, [Entropy](#) **24**, 10.3390/e24060841 (2022).

[23] G. Carrara, G. Murta, and F. Grasselli, [Phys. Rev. Appl.](#) **19**, 064017 (2023).

[24] Y.-M. Xie, Y.-S. Lu, Y. Fu, H.-L. Yin, and Z.-B. Chen, [Communications Physics](#) **7**, 410 (2024).

[25] Y.-S. Lu, H.-L. Yin, Y.-M. Xie, Y. Fu, and Z.-B. Chen, [Reports on Progress in Physics](#) **88**, 067901 (2025).

[26] M. Proietti, J. Ho, F. Grasselli, P. Barrow, M. Malik, and A. Fedrizzi, [Science Advances](#) **7**, eabe0395 (2021).

[27] A. Pickston, J. Ho, A. Ulibarrena, F. Grasselli, M. Proietti, C. L. Morrison, P. Barrow, F. Graffitti, and A. Fedrizzi, [npj Quantum Information](#) **9**, 82 (2023).

[28] K.-X. Yang, Y.-L. Mao, H. Chen, X. Dong, J. Zhu, J. Wu, and Z.-D. Li, [Phys. Rev. Lett.](#) **133**, 210803 (2024).

[29] Y. Du, Y. Liu, C. Yang, X. Zheng, S. Zhu, and X.-s. Ma, [Phys. Rev. Lett.](#) **134**, 040802 (2025).

[30] H. Liu, W. Wang, K. Wei, X.-T. Fang, L. Li, N.-L. Liu, H. Liang, S.-J. Zhang, W. Zhang, H. Li, *et al.*, [Phys. Rev. Lett.](#) **122**, 160501 (2019).

[31] W. Wang, F. Xu, and H.-K. Lo, [Phys. Rev. X](#) **9**, 041012 (2019).

[32] X.-Y. Zhou, C.-H. Zhang, C.-M. Zhang, and Q. Wang, [Phys. Rev. A](#) **99**, 062316 (2019).

[33] X.-L. Hu, C. Jiang, Z.-W. Yu, and X.-B. Wang, [Phys. Rev. A](#) **100**, 062337 (2019).

[34] F. Grasselli, Álvaro Navarrete, and M. Curty, [New Journal of Physics](#) **21**, 113032 (2019).

[35] W. Wang and H.-K. Lo, [New Journal of Physics](#) **22**, 013020 (2020).

[36] X. Zhong, W. Wang, L. Qian, and H.-K. Lo, [npj Quantum Information](#) **7**, 8 (2021).

[37] H.-T. Zhu, Y. Huang, W.-X. Pan, C.-W. Zhou, J. Tang, H. He, M. Cheng, X. Jin, M. Zou, S. Tang, *et al.*, [Optica](#) **11**, 883 (2024).

[38] Z. Zhang, Q. Zhao, M. Razavi, and X. Ma, [Phys. Rev. A](#) **95**, 012333 (2017).

[39] Y. Huang, Z. Du, and X. Ma, [Advanced Quantum Technologies](#) **7**, 2300275 (2024).

[40] M. Minder, M. Pittaluga, G. L. Roberts, M. Lucamarini, J. F. Dynes, Z. L. Yuan, and A. J. Shields, [Nature Photonics](#) **13**, 334 (2019).

[41] B.-Y. Tang, B. Liu, W.-R. Yu, and C.-Q. Wu, [Quantum Information Processing](#) **20**, 113 (2021).